J Mol Model (2003) 9:217–224
DOI 10.1007/s00894-003-0127-z

ORIGINAL PAPER

Krzysztof Murzyn · Marta Pasenkiewicz-Gierula

Construction of a toroidal model for the magainin pore

Received: 30 October 2002 / Accepted: 24 February 2003 / Published online: 27 May 2003

Abstract Magainins are natural peptides that selectively kill bacteria at concentrations that are harmless to animal cells. Due to a positive charge and distinct hydrophobic moment, magainins in the α-helical conformation interact favorably with bacterial membrane lipids. These interactions lead to the formation of large openings in the membrane and to the cell's death. The openings (toroidal pores) are supramolecular structures consisting of lipid and peptide molecules. A computer model of the pore in a bacterial membrane was constructed (see Figure) for the study of the molecular basis for magainin selectivity and specificity. Details of the construction and the preliminary equilibration of the pore model are given in this paper.

Keywords Antibacterial peptide · Magainin · Toroidal pore · Phosphatidylglycerol · Phosphatidylethanolamine · Lipid membrane

Abbreviations *M2a:* magainin-2 amide · *POPE:* 1-palmitoyl-2-oleoyl-phosphatidylethanoloamine · *POPG:* 1-palmitoyl-2-oleoyl-phosphatidylglycerol

Introduction

Magainins are short cationic peptides isolated from the skin of an African clawed frog *Xenopus laevis*. [1] They show both antibacterial and anticancer activity but are not hemolytic. In lipid membranes, they form α-helices of a distinct hydrophobic moment. [2] It has been shown that magainins disturb the structure of the lipid matrix of biomembranes. The extent of this disturbance depends on the lipid composition of the membrane. [3]

K. Murzyn · M. Pasenkiewicz-Gierula (✉)
Institute of Molecular Biology and Biotechnology,
Jagiellonian University,
ul. Gronostajowa 7, 30387 Kraków, Poland
e-mail: mpg@mol.uj.edu.pl
Tel.: +48-12-252-6518
Fax: +48-12-252-6902

Extended studies have been carried out to elucidate the molecular basis for the antibacterial activity and specificity of magainins. [4, 5, 6, 7] These studies are particularly attractive in view of the growing resistance of pathogenic bacteria to conventional antibiotics. A better understanding of factors that determine the mode of action of magainins will deepen our knowledge of the relationships between peptide structure and antibacterial activity, hopefully leading to the discovery of a new class of potent and specific peptide antibiotics able to overcome the deficiencies of presently used antibiotics. It should be noted that a highly basic magainin derivative, MSI-78, has already completed clinical trials for infected diabetic foot ulcers. [7]

Recently, a toroidal (or wormhole) model for magainin pores in the bacterial membrane has been proposed on the basis of in-plane neutron scattering data [8] and measurements of the lipid flip-flop rate. [9] The structure of the toroidal pore (Fig. 1a, b) emerging from experimental studies is highly complicated. The pore is built of peptide and lipid molecules. Lipids interpose magainin helices oriented perpendicular to the membrane surface such that the polar faces of the amphiphilic helices and the polar heads of the lipids constitute the pore lining. As a result, both membrane leaflets form a continuous surface, which allows for free diffusion of lipids between the outer and inner membrane layers. Such diffusion within the membrane of a living cell destroys the physiologically important asymmetry in the lipid composition of both membrane layers. [10, 11] While transmembrane movement of lipids may well be a signal that starts a cascade of potentially lethal reactions to a living cell, the formation of large openings in the membrane leads to its instant death.

The molecular dynamics (MD) simulation method is now accepted as an entirely reliable tool for the study of molecular systems of biological relevance. It requires a definition of the starting structure of the system at atomic resolution. The three-dimensional structure of proteins can be provided by experiments, which on the other hand do not offer a sufficiently detailed description of lipid

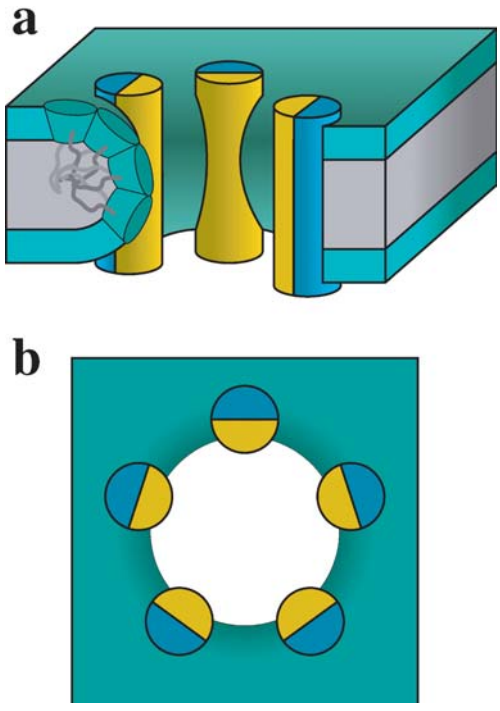

Fig. 1a, b The toroidal model for the magainin pore. The cross-section (**a**) shows: the interior of the pore with toroidal bending of the membrane surface (in *green*); peptide molecules as cylinders with polar face in *yellow*; and nonpolar in *blue*. **b** A top view of the pore. The packing of individual lipid molecules (headgroups depicted as cut cones, hydrocarbon tails as *dark gray* and *black* lines) in the region of toroidal bending of membrane (**a**) is also shown

bilayers. Such a description is often limited to a small set of parameters, e.g. the width of the membrane, the surface area per lipid molecule, the number of conformational defects in hydrocarbon tails of phospholipids, and so on.

The established view on a biological membrane is based on the Singer–Nicolson fluid mosaic model, [12] where the lipid matrix of a biologically active plasma membrane is in the liquid crystalline phase. This model, however, fails to describe numerous cellular processes, such as membrane fusion, endo- and egzocytosis among others. In the last several years, it has become obvious [13, 14] that transient non-lamellar phases in bio-membranes play an important role in these phenomena, indicating that biological membranes are morphologically variable and highly dynamical structures.

To construct the initial structure of a lipid bilayer for MD simulation, various strategies have been proposed in the past. [15, 16, 17, 18] The main concern of these strategies is that the bilayer reaches an experimentally characterized equilibrium state within less than a couple of nanoseconds. Unfortunately, there are no well-defined experimental parameters characterizing the equilibrium state of a complex, multi-component membrane system so, after insertion of peptides and other molecules into the bilayer as well as morphological disturbance of its structure, a very long simulation time is required to assure that the equilibrium state relevant for the nanosecond time scale is reached. To facilitate equilibration, the procedure of building the initial configuration of the system has to be carefully designed.

In this paper, the construction and a preliminary equilibration of the first computer model for the magainin pore in a bacterial membrane is described in detail. Subsequent MD simulation of the magainin pore will enable validation of the experimental hypotheses and hopefully will cast new light upon the factors leading to pore formation and stabilization.

Methods

Molecular composition of the membrane

A magainin pore forms in the bacterial membrane when the peptide to lipid ratio (*P*/*L*) is above 1:40. [19] The exact value of *P*/*L* depends on the lipid composition of the membrane and particularly on the content of anionic lipids. This indicates that, at least initially, the pore formation is an electrostatically driven process.

In the study of magainin pore formation and stability reported here, a computer model (called PORE) of the pore in a bacterial membrane was constructed consisting of magainin-2 amide (M2a), lipids, sodium ions and water molecules.

M2a is the most extensively studied representative of the magainin family. [7] At the physiological conditions, a +4 charge of M2a results from the positively charged N-terminus, four positively charged lysine residues and the negatively charged glutamic acid residue. The amphipathic character of the helical M2a molecule mirrors the helical wheel projection of the amino acid sequence (Fig. 2).

The lipid composition of PORE reflects that of a typical inner bacterial membrane. The membrane consists of zwitterionic 1-palmitoyl-2-oleoyl-phosphatidylethanolamine (POPE) and negatively charged 1-palmitoyl-2-oleoyl-phosphatidylglycerol (POPG) molecules in a 3:1 ratio. The structure and labeling of atoms in the lipid molecules is given in Fig. 3a–c. POPG and POPE are known to undergo numerous phase transitions depending on surface pH, temperature, and the concentrations of monovalent and divalent ions. This indicates a great flexibility in packing and space organization of phosphatidylethanolamine (PE) and phosphatidylglycerol (PG) molecules. These abilities might be of crucial

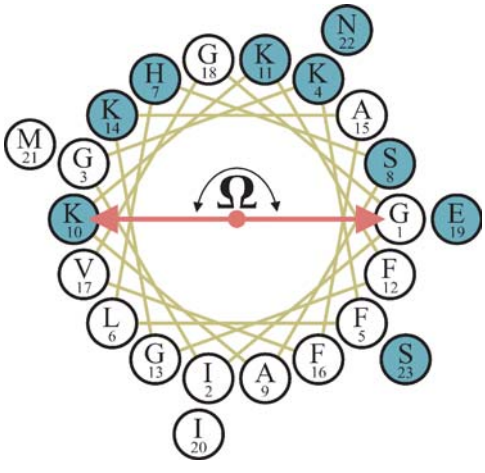

Fig. 2 M2a in the helical wheel projection. The polar and nonpolar aminoacid residues are shown in *green* and *white*, respectively. The Ω angle spans the polar face of the M2a helix

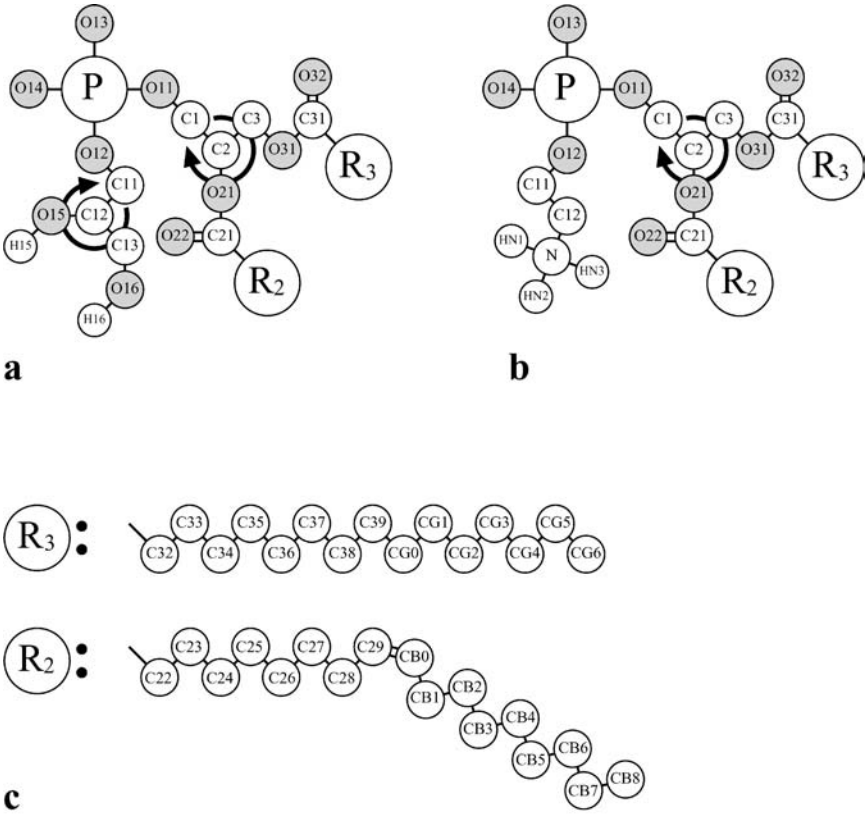

Fig. 3a–c Structure and numbering of atoms in phospholipids according to Sundaralingam. [33] The headgroup of **a** phosphatidylglycerol and **b** phosphatidylethanolamine. **c** The hydrocarbon chains R_2 (oleoyl) and R_3 (palmitoyl). *Arrows* in **a** and **b** circle chiral centers in POPG and POPG molecules

importance in promoting toroidal bending of membrane leaflets during pore formation by magainins.

PORE was hydrated with a sufficient number of water molecules and the electroneutrality of the whole system was ensured by the corresponding addition of sodium ions. A detailed description of the PORE system is given below.

Computational details

The project was carried out using the AMBER 5.0 package [20] for molecular mechanics (MM) and MD calculations and MSI Insight [21] for system construction. The secondary structure of M2a molecules was monitored with the DSSP program. [22] Visualization of the PORE structure and its building blocks was done with Rasmol, [23] Molscript, [24] and Raster3D [25] programs.

In MM and MD calculations, OPLS parameters for lipid [26] and peptide [27] molecules were used. Procedures for supplementing the original OPLS base with the missing parameters for the lipid headgroup have been described elsewhere by Pasenkiewicz-Gierula et al. [28] and those for the lipid β-chain sp^2 carbon atoms by Murzyn et al. [29] For sodium ions, Aqvist's parameters, [30] and for water, TIP3P [31] parameters were used. The united-atom approximation was applied to the CH, CH_2, and CH_3 groups of lipid and peptide molecules. The numerical values for atomic charges on POPE and POPG are given in [16]. To retain the double bond in the oleoyl chain of phospholipids in the *cis* conformation, restraints on the C28–C29–CB0–CB1 dihedral (cf. Fig. 3c) were imposed with a force constant of 100 kcal mol^{-1} rad^{-2}. Restraints acted whenever the deviation from an ideal conformation of 0° exceeded ±30°.

Chiral centers in POPE (atom C2, cf. Fig. 3b) and POPG (atoms C2 and C12, cf. Fig. 3a) molecules were kept in a chosen configuration by improper torsions: C1–C3–C2–O21 for C2 atom and C11–C13–C12–OC2 for C12 atom. The C2 center of naturally occurring POPE and POPG is in the R configuration (Cahn–Ingold–Prelog convention), whereas the C12 center in POPG is racemized. Both improper torsions were parameterized in the OPLS forcefield with half of the potential barrier equal to 14.0 kcal mol^{-1} rad^{-2}, a periodicity of 3 and the energy maximum at 0°.

The instantaneous orientation of the peptide molecules in the pore during preliminary equilibration and subsequent MD simulation was monitored using a rigid body quaternion fit as implemented in the MMTK package. [32] The reference helical structure of the M2a molecule was the experimentally determined peptide structure. [2] The helix was oriented in such a way (Fig. 4a, b) that its long axis coincided with the z-axis of the simulation box and the vector connecting the center of mass of sidechains located on the M2a polar face with the center of mass of the whole M2a molecule was parallel to the x-axis of the simulation box. The orientation of a peptide molecule in PORE was described relative to the reference structure with the two angles α and ϕ defined in Fig. 4c. The quality of superposition was tested by the root mean square deviation (RMSD) between the reference and a target structure.

Simulation conditions

Three-dimensional periodic boundary conditions with the usual minimum image convention were used. The SHAKE algorithm was applied to preserve the lengths of bonds involving hydrogen atoms, and the time step was set at 2 fs. For nonbonded interactions, a residue-based cutoff was employed with a cutoff distance of 12 Å. Subsequent MD simulation was carried out with the particle mesh Ewald (PME) method for treating long range nonbonded interactions. To reduce calculation time of nonbonded interactions in the cutoff scheme, each phospholipid molecule was divided into six residues; details are given in [16, 29]. The list of nonbonded pairs was updated every 25 steps.

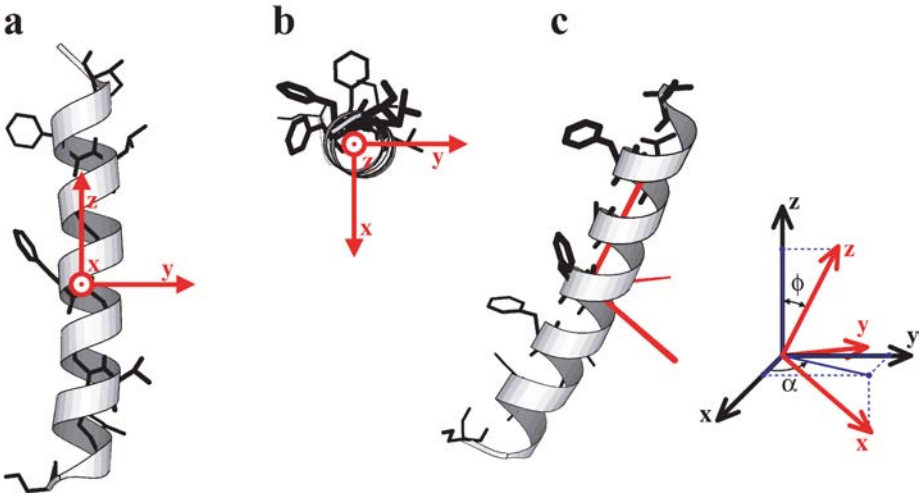

Fig. 4a–c The reference structure for M2a. **a** A side view, **b** the top view. Sidechains of residues located on the nonpolar face of M2a (cf. Fig. 2) are shown as sticks (the linewidth decreases with an increasing distance from the viewer). **c** Definition of α and ϕ angles used in the analysis of instantaneous orientation of the peptide molecules during F1 simulation (see text for details)

Results and discussion

System construction

PORE was constructed in several steps illustrated in Figs. 5a–e and 6a–e. At first, a supramolecular complex consisting of five M2a, 20 POPG and ten POPE molecules modeling the structure of the toroidal magainin pore was built. Five M2a molecules were placed vertically in the *x,y*-plane of the simulation box (the plane of the membrane), so that the long axes of the helices were parallel to the *z*-axis of the simulation box (the membrane normal). The polar face of each M2a molecule pointed toward the geometric center of the pore (p_0) and the center of mass of each peptide molecule was on the perimeter of a circle with center at p_0 and a radius r_0 of 25 Å (Fig. 5a, b). The initial structure of all five M2a molecules was the reference structure described above (Fig. 4a).

Next, a lipid cluster of two POPE and four POPG molecules (EG_4E, Fig. 5c, d) was formed and its five copies were placed between consecutive M2a molecules (Fig. 5e). The two outer POPE molecules in the EG_4E cluster were positioned in such a way that the distance between their phosphorus atoms was approximately equal to the width of the bacterial membrane and the line linking the atoms was parallel to the *z*-axis. Each of the four POPG molecules in the cluster was rotated by 30° relative to each other around an in-plane axis (Fig. 5c). The structure of EG_4E was optimized by potential energy minimization.

Then, a cluster of six POPE molecules forming a 3×2 bilayer (E_6, Fig. 6a, b) was built. After structure optimization, the cluster was placed on the hydrophobic side of each M2a molecule (Fig. 6c). The magainin pore constructed in this way consists of five M2a, 40 POPE, and 20 POPG molecules; its structure was optimized to remove bad van der Waals contacts.

In the next stage, the lamellar part of PORE was prepared. A cylindrical hole (Fig. 6d) was created in the large POPE/POPG bilayer system made of four copies of the well-equilibrated (after 14 ns of MD simulation) model for a bacterial membrane [16] by removing POPE and POPG molecules from the bilayer center. To reduce a relatively packed structure of the membrane, all interlipid distances in the plane of the membrane were enlarged by 30%. The magainin pore prepared in the previous stage (Fig. 6c) was inserted into the hole (Fig. 6d). Then, several POPE and POPG molecules were removed from the bilayer edges to reach a *P*/*L* ratio of about 1:40 and a

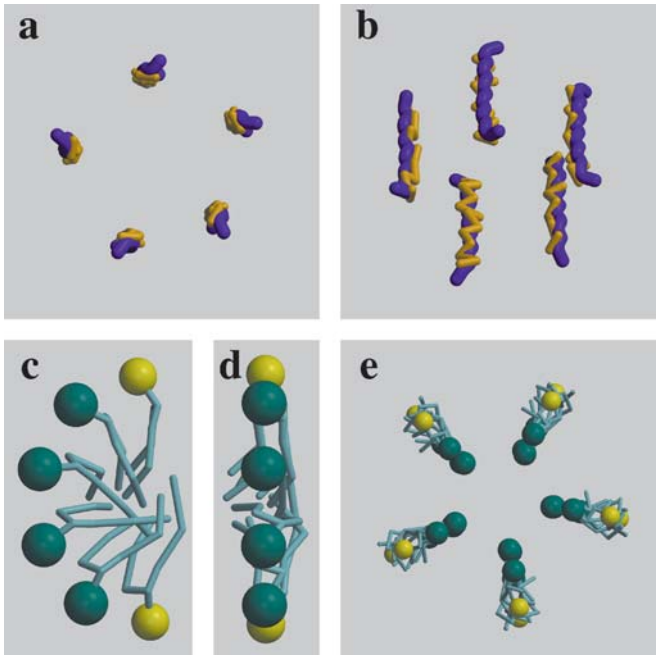

Fig. 5a–d Stages of PORE construction. **a** The top view and **b** a perspective view of 5 M2a helices (backbone shown in *purple*, the polar face in *gold*). **c** and **d** Side views of EG_4E cluster (see text for details). POPE and POPG lipid molecules in the cluster are shown schematically. The headgroup of POPE and POPG is shown as *yellow* and *green* spheres, respectively. The hydrocarbon tails are in *steel blue*. **e** The top view of five EG_4E clusters in the initial pore arrangement

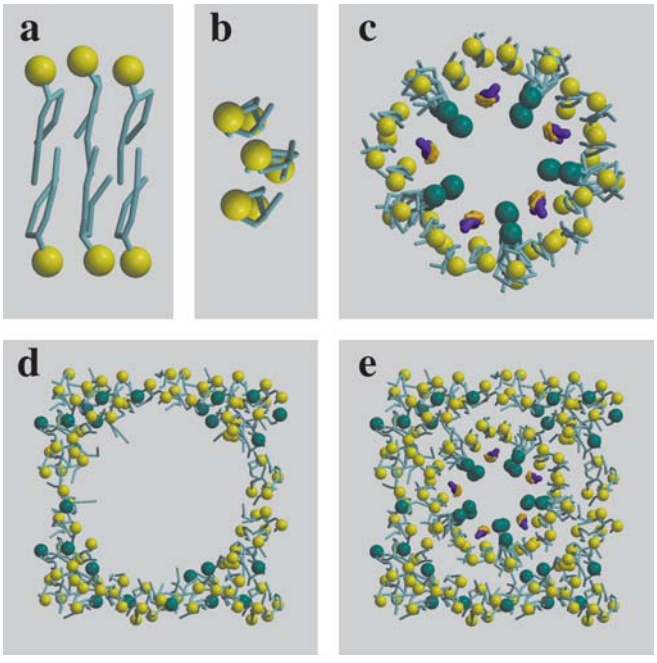

Fig. 6a–e Stages of PORE construction—continued. **a** A side view and **b** the top view of E_6 cluster (see text for details). The coloring scheme of lipid molecules is described in the caption to Fig. 5. **c** The top view of the magainin pore built of five M2a molecules (in *purple* and *gold*), five EG_4E clusters, and five E_6 clusters. **d** The top view of the lamellar part of PORE. The size of the hole in the bilayer center matches the size of the supramolecular complex shown in **c**. **e** The pore (**c**) is now placed in the central part of the bilayer (**d**)

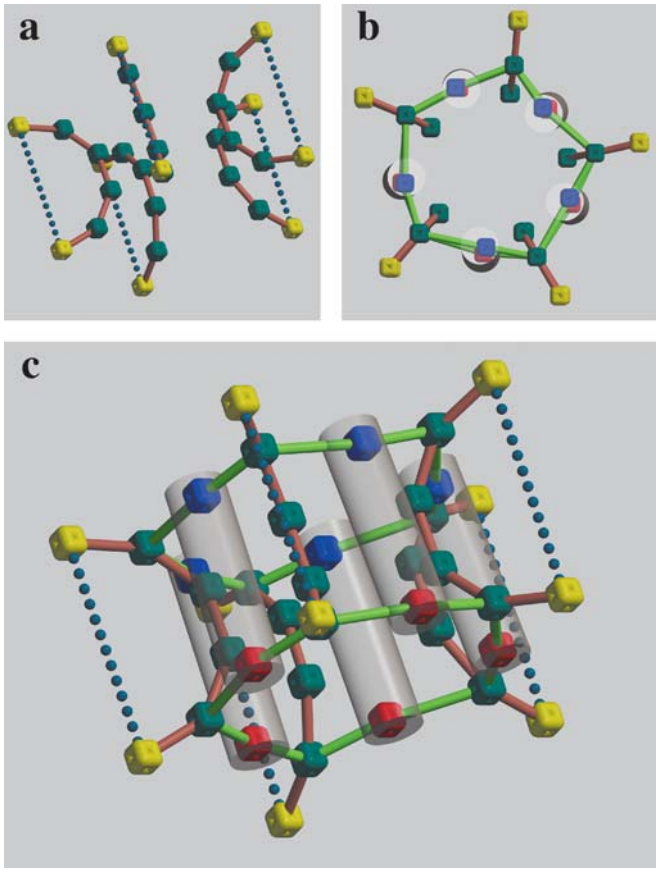

Fig. 7a–c Restraints in PORE. Restraints and their symbols are defined in Table 1. CM_{POPE} and CM_{POPG} are shown, respectively, as *yellow* and *green* cubes. CM_{GIGK} and CM_{IMNS} are shown, respectively, as *blue* and *red* cubes. **a** A perspective view of restraints imposed on lipid molecules in EG_4E clusters. The restraints of type CM_{POPE}-CM_{POPG} and CM_{POPG}-CM_{POPG} (see Table 1) are shown as *salmon solid* lines. The restraints of type CM_{POPE}-CM_{POPE} are shown as *dotted* lines. **b** The top view of restraints imposed for molecules forming the magainin pore. M2a molecules are shown as transparent cylinders. The restraints of type CM_{POPG}-CM_{GIGK} and CM_{POPG}-CM_{IMNS} are shown as *solid green* lines. **c** A perspective view

POPE/POPG proportion of 3:1. Eventually, the PORE system consisted of 138 POPE, 46 POPG and five M2a molecules (*P*/*L* ratio of 1:36.8).

Finally, PORE was immersed in the water box and the net charge of the system was compensated by adding 26 sodium ions (Na^+). After removing water molecules whose oxygen atom was within 4 Å of any atom of POPE, POPG, M2a, and Na^+, the total number of water molecules was 5,909 and the total number of all atoms in the system was 28,457.

The structure of the PORE system constructed as above was then optimized by potential energy minimization under three-dimensional periodic boundary conditions. Finally, the system was submitted to two-stage (F1 and F2) MD simulation, covering 250 ps and 100 ps, respectively.

Preliminary equilibration

To preserve the supramolecular structure of the magainin pore, a set of restraints keeping molecules in a given configuration was defined. The restraints kept the centers of mass of the atom groups in allowed ranges for the first 200 ps of F1 simulation. For restraints, the flat bottom potential (V_R) was used as defined and implemented in the AMBER package: [20]

$$V_R(r) = \begin{cases} 2k_2(r_1 - r_2)(r - r_1) + k_2(r_1 - r_2)^2, & r \le r_1 \\ k_2(r - r_2)^2, & r_1 < r \le r_2 \\ 0, & r_2 < r \le r_3 \\ k_3(r - r_3)^2, & r_3 < r \le r_4 \\ 2k_3(r_4 - r_3)(r - r_4) + k_3(r_4 - r_3)^2, & r_4 < r \end{cases} \quad (1)$$

where r_1, r_2, r_3, r_4 are limiting distances between selected groups and k_2 and k_3 are force constants.

The restraints, whose definitions are given in Table 1, are shown graphically in Fig. 7a–c. After 200 ps of F1 simulation, all restraints were released.

MD simulation of the first 10 ps was carried out at 10 K. During the next 100 ps, the temperature was slowly raised to 350 K and for a subsequent 100 ps it was lowered to 310 K, at which temperature the productive

Table 1 Definitions of restraints used in F1 simulation of PORE. See text for details. Distances r_1, r_2, r_3, r_4 and force constants k_2 and k_3 are defined in Eq. 1. CM_{POPE} and CM_{POPG} denote the center of mass of the headgroups of, respectively, POPE (Fig. 3b) and POPG (Fig. 3a). CM_{GIGK} and CM_{IMNS} denote the center of mass of, respectively, four N-terminal and C-terminal residues in M2a

Restraints type	Limiting distances (Å)				Force constants (kcal mol^{-2} Å^{-2})	
	r_1	r_2	r_3	r_4	k_2	k_3
CM_{POPE}–CM_{POPG}	1.0	9.0	12.0	20.0	10.0	10.0
CM_{POPG}–CM_{POPG}						
CM_{POPE}–CM_{POPE}	25.0	34.0	36.0	50.0	10.0	10.0
CM_{POPG}–CM_{GIGK}	10.0	13.0	15.0	18.0	5.0	5.0
CM_{POPG}–CM_{IMNS}						

Table 2 The largest (E_{pot}>1.0 kcal mol^{-1}) violations of restraints in PORE. The types of restraint are defined in Table 1. #R denotes the number of restraints of a given type defined in PORE. r denotes the distance between center of masses of particular atom groups. E_{pot} denotes the potential energy of restraints

Restraints type	#R	r (Å)	E_{pot} (kcal mol^{-1})
The onset of F1 simulation, 0 ps			
CM_{POPG}–CM_{POPG}	15	8.505	2.454
		8.669	1.093
		8.341	4.345
CM_{POPE}–CM_{POPE}	5	33.299	4.910
		32.429	24.670
		33.056	8.909
		33.314	4.710
		32.035	38.611
CM_{POPG}–CM_{GIGK}	10	12.445	1.541
		12.323	2.295
CM_{POPG}–CM_{IMNS}	10	12.425	1.653
Before removing restraints, 200 ps			
CM_{POPG}–CM_{POPG}	15	8.666	1.115
CM_{POPE}–CM_{POPE}	5	33.525	2.253
CM_{POPG}–CM_{GIGK}	10	12.390	1.860

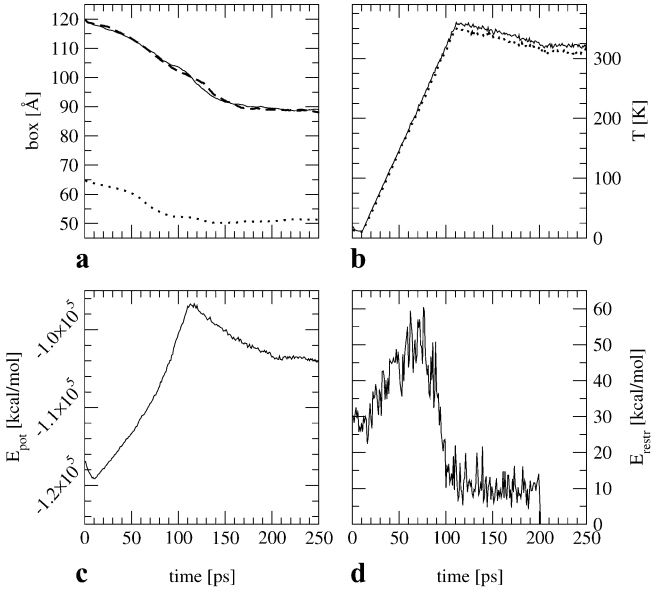

Fig. 8a–d Time profiles of control parameters in F1 simulation of PORE: **a** box dimensions (box), **b** temperature (T), **c** potential energy (E_{pot}), **d** the energy of restraints (E_{restr})

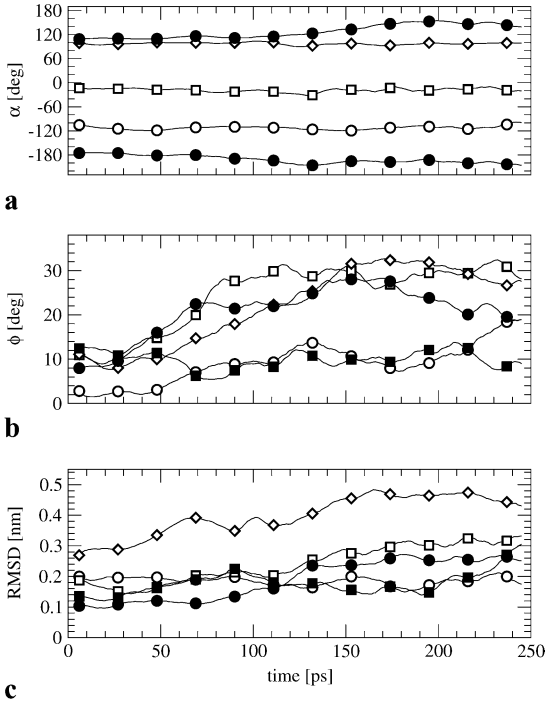

Fig. 9a–c Time profiles of **a** α, **b** ϕ angles, and **c** RMSD in F1 simulation. See text for details. Definitions of the angles are given in Fig. 4c

MD simulation was carried out (Fig. 8b). Time profiles of the simulation box size, the temperature, the potential energy (E_{pot}), and the energy of restraints (E_{restr}) during the initial equilibration are shown in Fig. 8a–d. Time profiles of α and ϕ angles (Fig. 4c) describing instantaneous orientations of M2a molecules in the pore and RMSD parameters describing their conformational changes are shown in Fig. 9. As can be seen from Fig. 8, the box dimensions and the potential energy quickly follow changes of the system's temperature. The shape of the E_{restr} profile (Fig. 8d) shows that all molecules involved in pore formation adjusted their relative positions to satisfy the imposed constraints. There is a significantly lower level of the violation of restraints at the end of the F1 simulation than at its beginning (Table 2).

Although in the course of F1 simulation M2a molecules altered their orientations with respect to the bilayer normal (ϕ angle, Fig. 9b), their polar faces

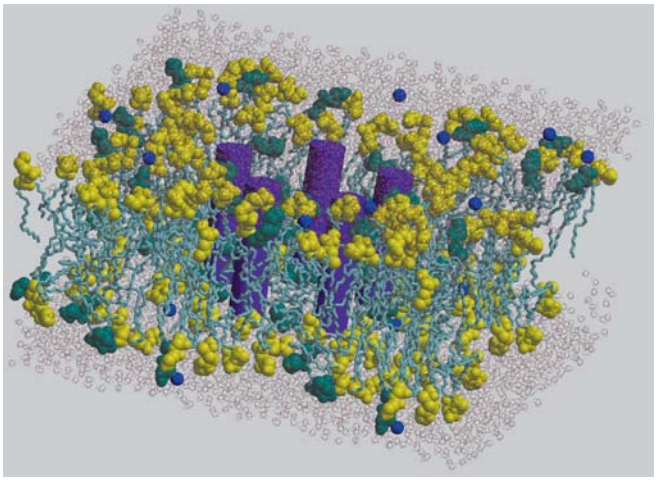

Fig. 10 The pre-equilibrated structure of PORE after F2 simulation. M2a molecules are shown as *purple* cylinders. Sodium ions are shown as *blue* spheres and the water molecules have no color. For lipids, the coloring scheme described in the caption to Fig. 5 was used

Table 3 Helicity of M2a molecules for three time points during F1 simulation of PORE

Peptide	Helicity (%)		
	0 ps	200 ps	250 ps
M2a-1	95	85	90
M2a-2	95	48	67
M2a-3	95	52	43
M2a-4	95	81	57
M2a-5	86	95	86

remained exposed to the aqueous interior of the pore (Fig. 9a). Reorientations were accompanied by some conformational changes (Fig. 9c), which resulted in lowering of the average helicity from 93% at the onset of simulation to 69% at its termination (Table 3).

Observed changes in the secondary structure of M2a molecules were, most likely, a consequence of a complex way the supramolecular system was constructed with several cycles of energy minimization and restrained MD simulation. These conformational changes could bias subsequent simulations, so the initial secondary structure of the peptide molecules was recovered. By optimal superposition of the reference and a target structure, all peptide molecules in PORE were replaced one by one. Thus, in the final configuration of PORE, all M2a molecules were fully helical and lipids both in the toroidal and lamellar parts of membrane were preliminarily equilibrated.

In a subsequent 100-ps MD simulation (F2) the structure of the magainin pore (five M2a and five EG_4E) was frozen by applying a belly F2 dynamics. The generated configuration of PORE (Fig. 10) served as an initial configuration in the 20-ns productive MD simulation, in which a different protocol employing the PME method for treating electrostatic long-range interactions was used. A detailed analysis of the PORE trajectory, which will be published elsewhere, indicated that the simulation box dimensions and the total potential energy stabilized within 3 ns but several parameters describing the structure and the dynamics of lipid and peptide molecules converged in shorter time periods. In particular, the average helicity of M2a molecules reached a stable value of about 80% within the first nanosecond of the productive run and the pattern of interactions between lipid and peptide molecules had established in 2 ns.

Conclusion

The first computer model for the toroidal magainin pore was constructed and preliminarily equilibrated. Further equilibration provided a system that was stable for the whole MD simulation time of 20 ns. Analyses of the trajectory generated in the productive run gave results that enable the identification of the molecular mechanisms responsible for antibacterial activity and specificity of magainin.

Acknowledgements This work was supported by grants 6 P04A 041 16, 6 P04A 031 21 and KBN/SGI ORIGIN 2000/UJ/048/1999 from the State Committee for Scientific Research and by European Union (contract no. BIER ICA1-CT-2000-70012). KM holds a fellowship award from the Polish Foundation for Science.

References

1. Zasloff M (1987) Proc Natl Acad Sci USA 84:5449
2. Gesell J, Zasloff M, Opella SJ (1997) J Biomol NMR 9:127–135
3. Matsuzaki K, Sugishita K, Fujii N, Miyajima M (1995) Biochemistry 34:3423–3429
4. Matsuzaki K (1999) Biochim Biophys Acta 1462:1–10
5. Tytler EM, Anantharamaiah GM, Walker DE, Mishra VK, Palgunachari MN, Segrest JP (1995) Biochemistry 34:4393–4401
6. Wieprecht T, Dathe M, Epand RM, Beyermann M., Krause E, Maloy WL, MacDonald DL, Bienert M (1997) Biochemistry 36:12869–12880
7. Maloy WL, Kari UP (1995) Biopolymers 37:105–122
8. Ludtke SJ, He K, Heller WT, Harroun TA, Yang L, Huang HW (1996) Biochemistry 35:13723–13728
9. Matsuzaki K, Murase O, Fujii N, Miyajima M (1996) Biochemistry 35:11361–11368
10. Herrmann A, Zachowski A, Devaux PF (1990) Biochemistry 29:2023–2027
11. Mollay C, Kreil G, Berger H (1976) Biochim Biophys Acta 426:317–324
12. Singer SJ, Nicolson GL (1972) Science 175:720–731
13. Cullis PR, de Kruijff B (1978) Biochim Biophys Acta 513:31–42
14. de Kruijff B (1997) Curr Opin Chem Biol 1:564–569
15. Pasenkiewicz-Gierula M, Takaoka Y, Miyagawa H, Kitamura K, Kusumi A (1997) J Phys Chem 101:3677–3691
16. Murzyn K, Pasenkiewicz-Gierula M (1999) Acta Biochim Pol 46:631–639
17. Cascales JJL, delaTorre JG, Marrink SJ, Berendsen HJC (1996) J Chem Phys 104:2713–2720
18. Lins RD, Straatsma TP (2001) Biophys J 81:1037–1046
19. Ludtke SJ, He K, Wu Y, Huang H (1994) Biochim Biophys Acta 1190:181–184

20. Case DA, Pearlman DA, Caldwell JW, Cheatham III TE, Ross WS, Simmerling CL, Darden TA, Merz KM, Stanton RV, Cheng AL, Vincent JJ, Crowley M, Ferguson DM, Radmer RJ, Seibel GL, Singh UC, Weiner PK and Kollman PA (1997) AMBER 5. University of California, San Francisco, Calif.
21. Insight II User Guide (1995) Biosym/MSI, San Diego, Calif.
22. Kabsch W, Sander C (1983) Biopolymers 22:2577–2637
23. Sayle R, Milner-White EJ (1995) Trends Biochem Sci 20:374–376
24. Kraulis PJ (1991) J Appl Crystallogr 24:946–950
25. Merritt EA, Bacon DJ (1997) Methods Enzymol 277:505–524
26. Jorgensen WL, Madura JD, Swenson CJ (1984) J Am Chem Soc 106:6638–6646
27. Jorgensen WL, Swenson CJ (1985) J Am Chem Soc 107:569–578
28. Pasenkiewicz-Gierula M, Takaoka Y, Miyagawa H, Kitamura K, Kusumi A (1999) Biophys J 76:1228–1240
29. Murzyn K, Róg T, Jezierski G, Takaoka Y, Pasenkiewicz-Gierula M (2001) Biophys J 81:170–183
30. Aqvist J (1990) J Phys Chem 94:8021–8024
31. Jorgensen WL, Chandrasekhar J, Madura JD, Impey RW, Klein ML (1983) J Chem Phys 79:926–935
32. Hinsen K (2000) J Comput Chem 21:79–85
33. Sundaralingam M (1972) Ann NY Acad Sci USA 195:324–355